The Orthogonal Transfer CCD[1,2]

John L. Tonry
Institute for Astronomy, University of Hawaii, Honolulu, HI 96822
Physics Dept., Massachusetts Institute of Technology, Cambridge, MA 02139
Electronic mail: jt@avidya.ifa.hawaii.edu

Barry E. Burke
Lincoln Laboratory, Massachusetts Institute of Technology, Lexington, MA 02173
Electronic mail: bburke@ll.mit.edu

Paul L. Schechter
Physics Dept., Massachusetts Institute of Technology, Cambridge, MA 02139
Electronic mail: schech@achernar.mit.edu

ABSTRACT

We have designed and built a new type of CCD that we call an orthogonal transfer CCD (OTCCD), which permits parallel clocking horizontally as well as vertically. The device has been used successfully to remove image motion caused by atmospheric turbulence at rates up to 100 Hz, and promises to be a better, cheaper way to carry out image motion correction for imaging than by using fast tip/tilt mirrors. We report on the device characteristics, and find that the large number of transfers needed to track image motion does not significantly degrade the image either because of charge transfer inefficiency or because of

[1]Observations in part from the Michigan-Dartmouth-MIT (MDM) Observatory.

[2]This work was sponsored by the Department of the Air Force and the University of Hawaii Consortium. Opinions, interpretations, conclusions, and recommendations are those of the author and not necessarily endorsed by the United States Air Force.

charge traps. For example, after 100 sec of tracking at 100 Hz approximately 3% of the charge would diffuse into a skirt around the point spread function. Four nights of data at the Michigan-Dartmouth-MIT (MDM) 2.4-m telescope also indicate that the atmosphere is surprisingly benign, in terms of both the speed and coherence angle of image motion. Image motion compensation improved image sharpness by about $0.5''$ in quadrature with no degradation over a field of at least 3 arcminutes.

1. Introduction

Light from a distant object passing through the atmosphere suffers phase distortions which cause an image of the object to dance and blur. These distortions are caused by turbulent density fluctuations in the air which translate to fluctuations in the index of refraction. The fluctuations are usually thought of as being stationary in time but blown across a telescope aperture by the wind, causing the wavefront of a point source to become a rapidly varying fractal landscape.

The Kolmogorov (1941) theory of turbulence has proved to be quite successful in describing how turbulence in the atmosphere leads to the temperature, density, and index of refraction variations which distort images. A classic text is Tatarski (1961), Parenti and Sasiela (1994) give a fairly recent and complete exposition, and Beckers (1993) provides an overview of adaptive optics. Briefly, turbulence of high enough Reynolds number has a self-similar behavior and transfers energy from an "outer scale" characteristic of the size where energy is fed into turbulent motions to an "inner scale" which is small enough that motions on that scale lose their energy to viscosity in a turnover time. Scaling arguments then require that the structure function D_n of index of refraction variations over this range of scales be given by

$$D_n = \langle (n(\vec{r}_1) - n(\vec{r}_2))^2 \rangle = C_n^2(h)\, r^{2/3},$$

where C_n^2 has units of $\mathrm{m}^{-2/3}$ and depends on height h above the ground, but locally the structure function depends only on the separation r of the points if the turbulence is isotropic and homogeneous.

The fact that the structure function increases rapidly with separation has two consequences. First, on a small enough scale (called r_0) the RMS distortions of the wavefront become less than a wavelength, and r_0 can be thought of as the largest aperture which is diffraction limited (albeit with substantial image motion) for given seeing conditions. The second is that without compensation there is virtually no improvement in image quality as a function of telescope aperture, since the contributions from the many subapertures of size r_0 have no long-term phase coherence.

There are many ways to characterize image quality; one of the most common and robust is the full width half maximum (FWHM) of a point source. Typical seeing might have a FWHM of $1''$ at 5000Å, corresponding to an r_0 of about 10 cm. When an aperture is larger than r_0, the light from all the r_0 sized subapertures interferes at the focus to produce a rapidly changing speckle pattern whose overall size corresponds to the diffraction pattern of a single r_0, but which carries fringes and speckles corresponding to the diffraction limit of the entire aperture.

Correcting the wavefront to recover the diffraction limited performance of an aperture is known as adaptive optics, and it requires phase corrections for each r_0 sized subaperture of the telescope, on time scales which are roughly the time it takes the wind to blow a distance of r_0, i.e. milliseconds. The difficulty is knowing the phase error of each subaperture, which requires we collect perhaps 100 photons per subaperture per correction time. This is evidently independent of telescope aperture, and steeply dependent on r_0. A star of $m = 7.5$ issues about 1 photon per Å per second per cm^2, hence we require a star (natural or artificial) of

$$m \approx 8 + 7.5 \log(\frac{r_0}{10\mathrm{cm}}) - 2.5 \log(\frac{v}{25\mathrm{m/s}}), \quad (1)$$

assuming a 3000Å bandpass, a 50% quantum efficiency, two samples per transit time, and no detector noise.

A related problem is that of the "isoplanatic angle," the angle over which phase distortions are substantially the same. In the context of this simple model we might expect this to be $\theta \approx r_0/h$, where h is the altitude where the phase distortions are taking place. This angle is small: for $r_0 = 10$ cm and $h = 2$ km, $\theta = 10''$. If the distortions are all occurring at a single altitude it is possible to conjugate them onto the device making the phase corrections and thereby greatly increase this isoplanatic angle, but this is seldom the case.

Finding a natural star which is bright enough and near enough to a target of interest is such a demanding requirement that attention has turned to the possibility of laser beacons, adaptive optics in the infrared (the index of refraction becomes slightly smaller but mostly the phase distortions are fewer wavelengths, hence r_0 becomes dramatically larger, perhaps as large as a meter at 2μm), or incomplete correction of phase distortions by correcting over a scale much larger than r_0.

This last option is the natural one to choose when we can profit from any improvement in image sharpness, when we require observations in the optical, and when we have a finite budget and lifetime. There are a number of projects which fit this description; two which we have been involved in are surface brightness fluctuations where the darker skies and quality of optical detectors are important (see Jacoby et al. 1992 or Tonry et al. 1997 for a review), and photometry of close gravitational lenses to search for time delays, where the fluctuations in QSO luminosity are greater in the optical (e.g. Schechter et al. 1997).

The usual approach in this incomplete correction of the wavefront is to decompose the wavefront into modes, usually Zernicke polynomials which are orthogonal polynomials on a circular disk, and correct for some limited number of modes. Effectively what we are doing is deliberately using an r_0 in the above formula which is just as large as we please, knowing that we will not be achieving diffraction limited performance, but hoping that there will be a worthwhile improvement in image quality. Evidently, this can lead to improvements in the requirements for brightness of guide stars, the speed at which we have to track the motion, and the angle over which the correction is effective.

For example, plugging $r_0 = 2.4$ m into the formulae above suggests that we should be able to work with $m = 18$ guide stars, that the rate at which we will have to track the motion might be 20 Hz for a 25 m/s wind, and that we can expect a correlation angle (usually known as the "isokinetic angle" when we are only talking about full aperture image motion) of 4 arcminutes for phase distortions at $h = 2$ km.

The lowest two modes we could consider are x and y gradients, colloquially known as "tip/tilt," and more precisely termed "G-mode" and "Z-mode" depending on whether we use an average of the gradient values over the wavefront or fit a least-squares gradient to the wavefront (the two lowest Zernicke terms). These modes correspond to image motion: the entire speckle pattern dances around with some amplitude. Since r_0 is defined as a subaperture over which there is roughly one wavelength of wavefront distortion, we can expect that a single subaperture will have a motion FWHM of $\Delta\alpha_1 \approx \lambda/r_0$, i.e.

very similar to the FWHM from diffraction.

If the structure function were not rising as a function of separation, we would see a reduction in image motion inversely proportional to telescope aperture D, because of the averaging of the positions of the images from each subaperture. However, the extra power at large scales causes the image motion to decrease only as $D^{-1/6}$, i.e. it is always comparable to the diffraction size of a single r_0 subaperture. Thus it is always important to remove the image motion from the atmosphere as well as image motion from telescope shake.

There have been a number of instruments built to compensate for image motion. Some of the more successful have included ISIS (Thompson and Ryerson 1984), the HR-Cam at the CFHT (McClure et al. 1989) and its successor the MOS/SIS, the COME-ON AO system (which is capable of higher order correction than just tip/tilt) at ESO's NTT (Rigaut et al. 1991), and various tip-tilt secondaries (Steward 90-in, UH 2.2-m, OCIW 2.5-m at Las Campanas). These work by incorporating a mirror into the light path which can be rapidly tilted to steer the light, either a small mirror in a reimaged beam, or the secondary of the telescope itself. A novel approach carried out by McCarthy et al. (1997) is to mount the detector itself on piezoelectric actuators and shake the focal plane. The challenge with all of these devices is to make the moving element light and stiff enough to push resonances to high enough frequencies that it is possible to maintain a stable control loop at 20–50 Hz. This is not an insignificant engineering achievement and it is generally quite expensive to do, particularly the most ambitious projects where the telescope secondary is articulated.

The gains from using these devices can be significant. Not only can image motion from the atmosphere be frozen, but also any telescope shake can be removed. Nevertheless, these devices are often difficult to use, offer small gains, and cause enough degradation in images (loss of light, non uniform PSF, setup overhead) that most images taken today do not benefit from image motion compensation, other than using a standard autoguider sampling at rates less than 0.5–1 Hz.

We have embarked on a project to achieve image motion compensation in a somewhat different way, by moving the electrons within a CCD to follow the optical image falling on the device. This is a new type of CCD, which we call an orthogonal transfer CCD (OTCCD), designed and built at MIT Lincoln Laboratory, which substitutes a fourth gate for the usual channel stop, hence permitting side-to-side parallel clocking of charge as well as up and down. (Ken Freeman has coined the acronym MIAOW for minimum inertia adaptive optics widget.) Our first device was only 64×64, but demonstrated that the concept works and that it is possible to shift a developing image within a CCD to any position (Burke et al. 1994). We have since built a 512×512 device with equal size frame-store region, and we have collected engineering and scientific results at the telescope with it. The advantages of this device are that it can shift charge *much* faster than an optical image is likely to move (within $\approx 100\mu$sec), it suffers from none of the problems incurred with moving optics, and it is an extremely cheap option to build into a CCD.

The next section will describe the device in more detail, along with how it is actually used at the telescope. The third section will discuss the main drawback to this device: pockets and traps create holes in images when the

charge has been shifted back and forth many times. The fourth section will present results from four nights of use in July 1996 at MDM Observatory. We report on the significant improvements in image quality using this device. We will then conclude and speculate on directions for its future development.

2. Structure and Use of the OTCCD

Figure 1 shows a schematic diagram of the gates overlaying a pixel in the OTCCD, and a photomicrograph of an actual device. In a normal CCD the fourth phase would be a channel stop implant, whereas in the OTCCD the channel stops are small implants at the corner of each pixel. If this fourth phase is set low, however, it acts like a conventional channel stop and we can clock the charge in the device down with the 3-phase sequence 1–2–3–1 or up with the sequence 1–3–2–1. However, we have also altered the geometry of the two central phases, 1 and 2, into triangles which are rotation symmetric, and the third phase is symmetric with phase 4, so that we can also clock charge left and right. This is achieved by setting phase 3 low and using the sequences 1–4–2–1 for right movement or 1–2–4–1 for left movement. For normal integration we set both phase 3 and phase 4 negative and collect under phases 1 and 2.

The first realization of this geometry was a 64×64 test device which worked as expected (Burke et al. 1994), but was too small for effective tests of charge transfer inefficiency (CTI) or rate of incidence of pockets and traps. Fortunately, the chords of a mask set for another CCD development program became available at this time, and we seized the opportunity to build a larger OTCCD. (The other program only used the square inscribed within the circular wafers.)

In order to make a device which could track image motion without any external inputs, we decided to build a chip with a 512×512 array of OT gates and a 512×512 array of conventional 3-phase gates. This lower portion of the chip could be used as a frame-store area, but we chose to leave it uncovered so that it could be used to track a guide star. Both arrays dump into a split serial register with amplifiers at each end. We wanted this CCD to be as simple as possible to use, so we kept the number of clocks to 12 so that the OTCCD could be run with a single SDSU/Leach analog board (4 OT gates, 3 three-phase gates, 3 serial gates, a summing well, and reset). The pixels are 15 μm which translates to $0.17''$ at the Michigan-Dartmouth-MIT (MDM) 2.4-m telescope, and the entire chip is therefore $1.5' \times 3'$.

Because of financial constraints and because we did not want to introduce any processing which might jeopardize the standard three-phase devices on the same wafer, we chose to use aluminum for the topmost gate (number 1). As we discovered, this may have increased the incidence of pockets.

Figure 2 illustrates how the OTCCD is operated at the telescope. The telescope is first positioned to place the field of interest on the OT region of the chip. Next, a suitably bright guide star is sought, possibly by rotating the instrument. For the observations in July we were using a front-side illuminated device (where aluminum covers about 60% of the chip), so the quantum efficiency was low. A star of $m_I \approx 23.5$ gave us $1e^-$/sec through a standard Kron-Cousins m_I band filter, and we could track at 10 Hz on stars of about $I = 15.5$. The probability of finding a star within the $1.5'$ field at this brightness is about 0.6 at the north galactic pole, so for

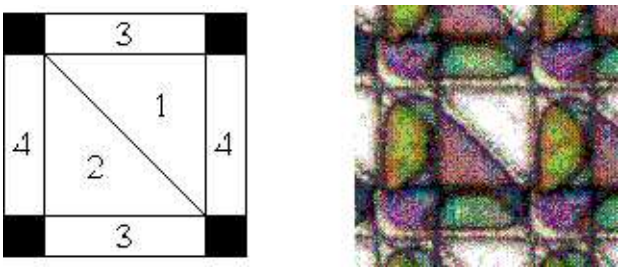

Fig. 1.— On the left is a schematic of how the four gates of an OTCCD are organized. On the right is a photomicrograph of an OTCCD pixel. In this device gate #1 is aluminum and therefore appears bright.

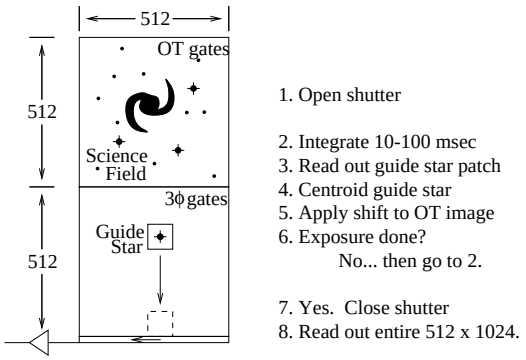

Fig. 2.— The OTCCD is used to track image motion by placing the science field on the portion of the CCD with OT gates and a guide star on the frame-store portion of the CCD. A subarray containing the star image is rapidly read out and used to correct the position of the charge within the OT array to follow the motion of the science field.

some fields we had to track more slowly than 10 Hz. The back-side illuminated devices currently being fabricated will improve this by about 1.5 magnitudes and we can improve the signal to noise of our guide star detection by about a factor of 2 (another 0.7 mag), which will bring the probability of finding a guide star for 10 Hz within $1.5'$ to greater than 0.9.

We use our technique of "shutterless video" (Metzger, Tonry, and Luppino 1993) to read out guide star information while the OTCCD is integrating on the science field. This method is applicable to any CCD, whether or not it has a shadowed frame store area (the OTCCD does not), and it is the usual means at MDM to focus the telescope and examine out of focus donuts for miscollimation. The shutterless video and the resulting image tracking loop are illustrated in Figure 2.

This method has some shortcomings compared to a device with a real frame store: there is a bit of vertical streaking from the star as the charge is clocked past, the guide star subarray must be at least one subarray size above the serial register, it is possible to have ghosts if there happens to be a bright object above the serial register where the guide star image is being read out, and there is some of loss of duty cycle because the time while the image is read out (≈ 4 msec for a 16×16 patch) cannot be used for integration. On the other hand, it is possible to select an arbitrary guide star region with arbitrary binning, and this can be used with any CCD.

The choice of where to move the charge collecting in the OT region as a result of the guide star information is an interesting exercise in control theory. In this case we have quite accurate information of guide star location (mostly good to a fraction of a pixel) extending into the past, but of course the

information is always one sample time late. The device we are controlling (the electrons in the OT region) has ideal properties: there is no inertia or backlash and we carry out the OT shifting in about 80 μsec per pixel (and a typical shift is only one pixel). Some algorithms which we have considered are (1) prediction = previous position, (2) prediction = linear extrapolation of previous positions, and (3) linear predictive coding or Kalman filtering of the previous positions. (Numerical Recipes by Press et al. 1992 has a short section on LPC and references to some of the standard engineering textbooks.) Algorithm #1 is pretty poor for a sinusoidal motion sampled at the Nyquist frequency, but algorithm #2 is even worse. We do not have much experience with algorithm #3 yet; in the lab it usually does spectacularly well, but is computationally expensive. All of the observations presented here are algorithm #1 with a "veto" limit on how large a shift a sample can call for.

Ideally we would like to optimize the tradeoffs between signal to noise and tracking speed, but whatever algorithm we select must be quite fast (computing in less than a few msec on a Sparc 2). We also require that the algorithm be extremely robust, because we only read out a small patch around the guide star and adjust the location of the subarray for the next sample according to where we think the guide star will be, so we cannot afford to have a bad sample or cosmic ray throw us off by more than a subarray size. This is quite a well defined problem in mathematics and control theory, and we would welcome suggestions on optimal algorithms.

As the observation proceeds, each of the guide star images is piped to a display which also shows the current centroid, a leaky average of the guide star images, and a strip chart of the image FWHM. One of the nice features about the OT tracking is that if the telescope focus drifts the observer can refocus in real time without worrying about causing the image to move.

When the exposure has finished the entire CCD reads out and the science image in the OT region is saved to disk. We also save a complete record of time, guide star position, and image shifts for each guide sample. This is necessary for creating a flat field because the science image has been dithered over many OTCCD pixels. If requested, the software will also record a 3-dimensional FITS file of the actual guide star images, and this movie can be replayed or analyzed for information other than centroid.

We have also written software to read one of these records of image shifts created during an exposure and to replay it at arbitrary speed. We thought this would be a better way to make a flat field: an image's actual shifts could be reproduced while the OTCCD is viewing a flat field and the pocket-pumping would occur in the same way. As we learned, however, this is both ineffective and unnecessary.

Presently we use the OT guide star information purely for OT tracking, and we depend on the usual telescope autoguider to guide the telescope. This is purely a matter of expediency and we can probably improve performance a bit (as well as making the observer's job simpler) by using a suitably filtered version of the OT guide star motion to move the telescope.

Since we had only five weeks from the receipt of the first OTCCD until our first observing run (during which we had to build a focal plane, write DSP code to run the

OTCCD, characterize chips, write DSP code to do the OT shifting, write code for the Sparcstation to do the centroiding, exposure management, data recording, and image display), there are a number of improvements we would like to carry out. First and foremost, we are far from extracting optimal signal to noise from our guide star images. When we can control the telescope position from the Sparcstation we should be able to center and bin appropriately to do quadrature detection. The image display can be made much more useful for the observer: a full frame view mode and some sort of guide star subarray graphic would be helpful.

The most interesting improvement we would like to implement is some sort of fast autofocusing. A quadrature detection produces four numbers, call them A, B, C, and D (Figure 3). We get flux information from A+B+C+D, x guide signal from (A+C)−(B+D), and y guide signal from (A+B)−(C+D). If we deliberately introduce some astigmatism at 45° to the pixels, we can get a focus signal from (A+D)−(B+C). This is a well-known trick for CD players. In our case, by placing a cylindrical lens of the proper thickness and power above the CCD we can place the two astigmatic foci symmetrically about the nominal image plane so that the focus signal will be zero when the telescope is in focus.

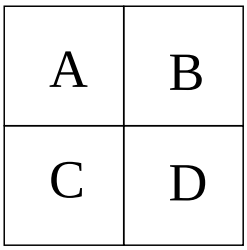

Fig. 3.— The four pixels of a quadrant sensor.

This focus signal could either be filtered and sent to the usual telescope focus mechanism, or it could be used to drive some fast focus adjustment, such as a tilting plate or a piezo drive of the focal plane itself.

3. CCD Performance and Pockets

3.1. Characterization in the Laboratory

We used iron-55 xrays and adjusted output FET drain voltage, V_{DD}, bias, and clock levels to optimize the CCD performance. Figure 4 shows the gain and noise level of the CCD as a function of V_{DD} at a frame rate of about 50 kpix/sec. At V_{DD} of about 20 V, the CCD amplifier puts out about 16μV per electron and achieves 1.6e^- noise.

A typical image taken with OT tracking will undergo 5000 shifts (perhaps 20 per second over a 250 sec exposure). We measure the CTI of the OTCCD to be better than 3×10^{-6}, which means that a charge packet might lose 1% of its charge into a surrounding halo during the course of an exposure. This is not a significant degradation of the point spread function.

The biggest concern about the viability of image motion compensation within an OTCCD was that traps or pockets might cause serious "pocket-pumping." For example, a bulk trap of only one electron depth might store an electron during each shift and release it later, potentially digging a 5000e^- hole in the image and building up a 5000e^- spike. Since typical exposures have sky levels of only a few hundred to a thousand electrons, this will seriously degrade the image. Early experiments by Stockman (1982) with RCA chips (and TI 800[2] CCDs also suffered badly from traps) indicated that this was a fatal problem for these

devices unless very few shifts were performed. Modern CCDs have far fewer traps and pockets, and have been used successfully for image chopping (e.g. Cuillandre et al. 1994 or Sembach and Tonry 1996), but we did not know how serious the problem would be with the OTCCD.

We experimented with deliberate pocket-pumping in the lab, either by shifting back and forth many pixels (at about 80μsec per shift) or by shifting back and forth by only two phases (to try to discover the subpixel location of traps). When the number of shifts was small enough that there were still electrons left in the afflicted pixel, we characterized the depth of the pocket as the depth of the hole or equivalently the size of the adjacent spike, and express the depth in units of electrons per clock cycle. We found that the number of pockets is quite variable from device to device, some having thousands of pockets bigger than $1e^-$, others with as few as a hundred. Figure 5 shows the distribution of pockets in one of the better devices. The number of pockets N depends roughly on pocket depth n_0 as $N \approx n_0^{-1/2}$.

The density of pockets in the OTCCD region of the best devices is about three times higher than the 3-phase region on all the chips. For temperatures cold enough to have negligible dark current we saw little change in pocket number and size with temperature. The pockets did become fewer (and smaller) as we clocked more slowly, but we needed a geometric increase in parallel transfer time to obtain a linear improvement in pocket size. The pockets are extremely sensitive to clock voltage: the bigger the voltage difference between adjacent phases during clocking, the smaller the pocket size. We could set the parallel clocks as negative as -10 V (although

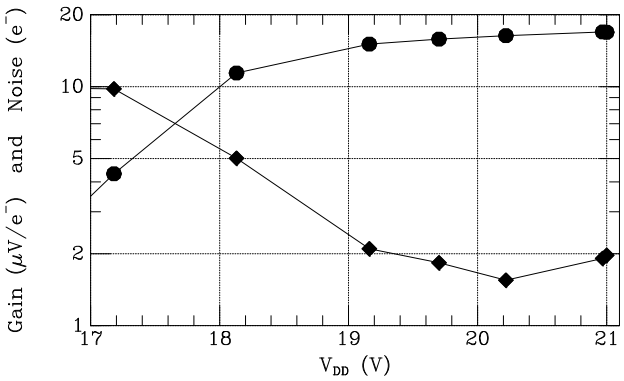

Fig. 4.— The read noise (declining curve) and responsivity (rising curve) of the OTCCD output amplifier as a function of drain voltage.

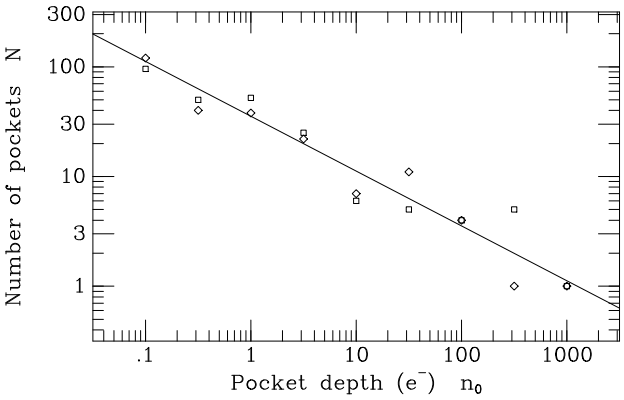

Fig. 5.— The number of pockets as a function of the pocket depth (determined by pocket pumping at a rate of 80μsec per shift). The squares and diamonds refer to pockets which trap charge when it is clocked up-down or left-right.

the surface potential pins around −6 V), and we found that we could not set the parallels more positive than about +4 V, without incurring some breakdown between the parallel and serial clocks. Apart from these general observations, we have not yet carried out detailed, quantitative characterization of pocket size as a function of all the various parameters.

A striking feature of these pockets is that they are virtually all unidirectional, i.e. they block the passage of a bit of charge in one direction, but do not impede charge in the other direction, a bit like water flowing over a curbstone. Generally speaking, the pockets trap charge when clocking either up or to the right, although some (and many of the larger ones) will trap charge when clocking down or left.

All of these considerations suggest that the pockets are localized electrostatic potential minima. The up-right (U-R) and down-left (D-L) unidirectionality of the trapping also points to something to do with the 45° interface between the 1 and 2 phases. This will be examined in more detail below.

3.2. Performance at the Telescope

The OTCCD performed well when we put it on the MDM 2.4-m telescope. What was surprising, however, was the fact that the pockets were much less pronounced than we had feared. Figure 6 shows an image of NGC 6703 at a contrast level to show 1% deviations from the sky level. There about 20 pockets apparent, but the rest are nearly invisible. Figure 7 shows the size of the pocket (in e^- per transfer) measured in this image versus the pocket size measured in the lab. Each pocket which we had measured in the lab was about a factor of 30 less prominent in

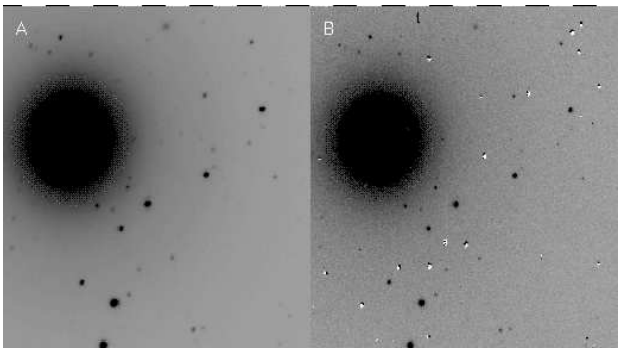

Fig. 6.— Two images of NGC 6703. The left image (A) was taken with a Loral CCD using normal guiding, and had an equivalent exposure of 5000 sec. The right image (B) had 4650 shifts during a 500 sec exposure. The PSF FWHM is 0.82″ on the left and 0.58″ on the right. The stretch is adjusted to make the pockets stand out.

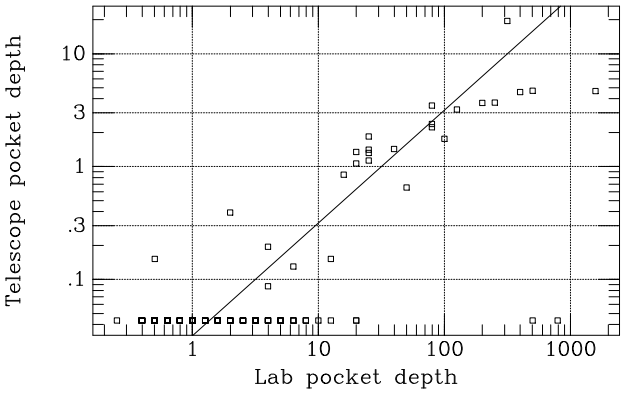

Fig. 7.— The size of pockets in images derived during actual observing is plotted against the size of the same pockets derived from pocket pumping experiments in the lab. The line illustrates a factor of 30 reduction in size.

astronomical images taken at the telescope. Since the image motion RMS is about 2 pixels, the entire pattern that the pocket traces is about 50 pixels. This image underwent 4650 shifts and the sky level is about $850e^-$. Therefore a pocket which traps $3e^-$ per shift in the lab (and appears to trap only $0.1e^-$ per shift here) would dig a hole in this image of depth $4650 \times 0.1/50$ and just be visible at a level of 1% of sky, whereas without this diminution of pocket size it would cause a deep hole of 30% of sky.

Expecting that the pockets would create images that were littered with pits, we wrote software to replay the pattern of shifts from an image while the OTCCD was illuminated by a flatfield. Any pocket deep enough to dig down to the bias level could not be corrected, but we thought that this would remove the smaller pockets. It turned out, however, that such flatfields do not to a good job of mimicking the pocket patterns in the data. Generally speaking, a flatfield is much brighter than a sky image so the replay of the shift pattern happens much more rapidly than the data exposure, and the eventual image is also much brighter than the data. Our realization of how sensitive the pockets are to dwell time enables us now to understand why this procedure is not effective in removing pockets. It is conceivable that we could use these flatfield data and a physical model to correct for the effects of the pockets, but they comprise such a small fraction of the area (about a percent), that it is probably more effective to simply to move the telescope between exposures and delete the data affected by pockets.

3.3. Diffusive Draining of Pockets

We believe that our pockets are electrostatic potential minima, as discussed by Chatterjee et al. (1979). The thermal diffusion of charge out of a pocket is described by $J = -D\nabla n$, where J is the flux of electrons, D is a diffusion constant which depends on temperature, and ∇n is the gradient of the number density. If we approximate the pocket as a rectangular volume of width L and cross section A, the barrier width as ΔL, the barrier height as $\Delta\phi_0$ when the pocket is empty and $\Delta\phi$ when the pocket is partially filled with charge, and the number of electrons in the pocket as N (Figure 8), we have $dN/dt \approx JA$, $\nabla n \approx N/(AL)/\Delta L$, and $D \approx D_0 \exp(-e\Delta\phi/kT)$. Hence

$$\frac{dN(t)}{dt} = -\frac{D_0}{L\Delta L} N(t) \exp(-e\Delta\phi(t)/kT). \quad (2)$$

We can also relate the barrier potential to the number of electrons in the pocket via a capacitance: $\Delta\phi = e(N_0 - N)/C$, where N_0 is the pocket capacity. Thus,

$$\frac{dN(t)}{dt} = -k_1 N(t) \exp(-\frac{N_0 - N(t)}{N_{kT}}), \quad (3)$$

where $N_{kT} = kTC/e^2$ is the number of electrons necessary to change the potential in the pocket by kT/e and $k_1 = D_0/(L\Delta L)$ is the diffusion rate.

We estimate that the pockets and barriers are a modest fraction of a pixel size, so that $L \approx \Delta L \approx 2\mu$m, and the diffusivity in silicon is $D_0 \approx 30$ cm^2/sec, so $k_1^{-1} \approx 1$ nsec. The capacitance between the charge and the gate is 4×10^{-8} F/cm^2, or $C \approx 10^{-15}$ F for these pockets. At $T = -100$ C we have $kT \approx 15$ meV and $N_{kT} \approx 100\ e^-$.

At $t = 0$ we imagine that the pocket is full of charge, $N(0) = N_0$, and the charge then drains out. The solution to this equation is an exponential integral, but its approximate behavior is straightforward to describe. The

charge in a shallow pocket with $e\Delta\phi_0 \approx kT$ will lose its charge very quickly, but in a deep pocket with $e\Delta\phi_0 \gg kT$ the exponential term will dominate, and the charge will drain more and more slowly. For $t \ll k_1^{-1} \exp(N_0/N_{kT})$ (i.e. $N(t) \gg N_{kT}$) we can approximate the factor of N outside the exponential as the constant N_0 and integrate the equation to get

$$N(t) \approx N_0 - N_{kT}\ \ln(1 + \frac{N_0}{N_{kT}}\, k_1 t). \qquad (4)$$

However, our situation calls for quantities of charge much less than N_{kT}, and this last part of the draining is even simpler to describe. If we define $x = N(t)/N_{kT}$ as the number of electrons in the pocket in units of N_{kT}, a characteristic time scale $\tau = \exp(N_0/N_{kT})\, k_1^{-1}$, and a dimensionless time variable $s = t/\tau$, equation 3 becomes simply $dx/ds = -xe^x$. In the limit that $x \ll 1$ (i.e. the last fraction of N_{kT}), $e^x \approx 1$, and the solution is trivially $x(s) = e^{-s}$. Thus over a time scale of τ we will see a very rapid drop of charge down to a level of N_{kT}, and subsequently an exponential decay of the rest of the charge with time scale τ:

$$N(t) \approx N_{kT}\ \exp(-t/\tau) \qquad \text{for} \qquad t > \tau. \qquad (5)$$

We see a fairly uniform reduction of a factor of 30 in pocket size as we slow the pixel dwell time from $\approx$ 100μsec to $\approx$ 30msec, which can be plugged into equation (5) to give $1/30 \approx \exp(-30\text{msec}/\tau)$, or $k_1^{-1} \exp(N_0/N_{kT}) \approx$ 10msec, or $N_0/N_{kT} \approx 16$. Although the pockets have a large range of electron capacities, this constancy indicates that the barrier height $\Delta\phi_0$ is relatively constant, since $N_0/N_{kT} = e\Delta\phi_0/kT$, so $\Delta\phi_0 \approx 0.25$V and $N_0 \approx 1000e^-$ for a typical pocket.

3.4. Reducing the Incidence of Pockets

We have a number of clues about the origin of the pockets we see in the OT region of the CCD. We find that (a) pockets occur in perhaps 1 pixel out of 300, (b) this incidence is substantially higher under the OT gates than under the 3-phase gates, (c) pockets are almost all unidirectional, and horizontal trapping and vertical trapping are related in the sense that we would expect for transfer across the 45° boundary between phases 1 and 2 (pockets which trap charge moving down generally also trap charge moving left and likewise for up-right, which is the same sense as the diagonal interface between phases 1 and 2), (d) the pockets are very sensitive to clock voltages, and (e) the pockets reduce by about a factor of 30 when the dwell time in phases 1 and 2 is increased to 30 msec.

Our best model for understanding this is that occasionally a pixel will have an electrostatic pocket in the acute corners of phases 1 or 2 and the potential there looks like a hanging valley (i.e. steep barriers into adjacent phases and shallow barrier into the center of the triangle). Charge is very reluctant to be clocked out of this pocket into one of the adjacent phases, which gives rise to the pocket pumping. However, given enough time, the charge will slowly drain into the center of the phase from which it will readily move into a different phase. A simple physical analysis of the situation suggests that these pockets have a fairly constant barrier of 0.25 V, but vary greatly in physical size, capacitance, and capacity for electrons.

The low incidence of pockets indicates that this is not a true design flaw, but that occasionally something goes wrong and a pocket gets created. We are suspicious of the alu-

minum used for gate #1, since it is suspected of having small voids associated with hillock formation after the customary forming-gas (H_2/N_2) anneal. Processing can also cause aluminum to lift or be undercut, but examination of pocket-bearing pixels has not revealed this to be the case. Any nonuniformity in the separation between channel and gate can cause a pocket. Fabricating a device where the fourth level phase is polysilicon will permit us to test this hypothesis about the origin of the pockets.

4. The Atmosphere and Image Motion

4.1. Observations

Our first run with the OTCCD took place in July 1996, and the clouds relented long enough to collect data on four nights. During that time the seeing (guided but without OT tracking) ranged from 0.63″ to 1.27″, which is typical for the MDM 2.4-m telescope on Kitt Peak.

The device which we used has a rather low quantum efficiency because it is front-side illuminated and has more than half of each pixel covered by opaque aluminum. We found that we would collect 1 electron per second from a source of $m \approx 23.5$, but this will improve by about 1.5 mag when we have a back-side illuminated, antireflection coated OTCCD.

While removal of image motion by OT tracking is not true adaptive optics, and although we will never rival the performance of HST, we can obtain very significant improvements in scientific quality. Figure 9 illustrates the sort of improvement we achieved with OT tracking of image motion. The left panel shows an image of the globular cluster M71 with ordinary guiding when the see-

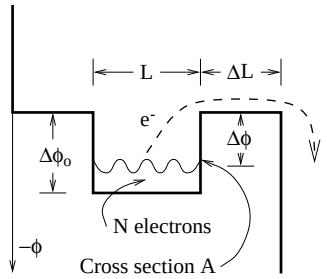

Fig. 8.— A pocket of volume $L * A$ has a potential barrier of height $\Delta\phi_0$ when the pocket is empty and width ΔL. Electons must overcome the barrier $\Delta\phi$ in order to escape from the pocket.

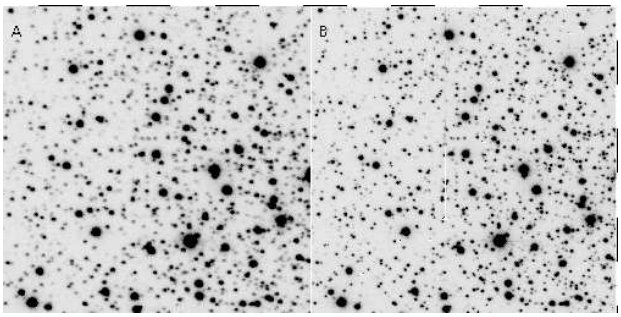

Fig. 9.— Two 150 sec images of M71 taken in immediate succession. The left one (A) used only normal guiding and has a PSF FWHM of 0.73″; the right image (B) had 1113 OT shifts applied and resulting images of 0.50″.

ing was quite good (0.73″). The right panel shows the improvement when we carry out OT tracking at 7 Hz (0.50″). Although the seeing was not always this good, we almost always achieved this level of improvement (describable as removal of 0.5″ in quadrature, or reduction in FWHM by 20%) over normal guiding by use of OT tracking. We took a number of pairs of exposures with normal guiding followed by OT tracking, and Figure 10 plots the FWHM with OT tracking against the FWHM with normal guiding, illustrating this level of improvement. Also shown on the plot is the FWHM motion of the image centroid observed during the observation. The dashed line demonstrates that this motion is roughly 0.6 times the FWHM.

Perhaps even more remarkable, we *never* saw any degradation of the PSF across the OTCCD, which implies that the motion of the guide star and science field must be very highly correlated across at least 2.5′. Figure 11 is a blowup of two regions of Figure 9, one from the lower part of the OTCCD which was about 0.5′ from the guide star, and the other from the upper part at 2.0′ separation. Figure 12 quantifies this by showing that the image FWHM does not vary significantly with distance from the guide star. The fit rises from 0.481″ at $r = 0.3'$ to 0.485″ at 2.3′, indicating (possibly) a contribution of 0.06″ in image size due to uncorrelated image motion.

A further clue to the origin of the image motion comes from its temporal behavior. Figure 13 shows a time series of (unguided) image motion in one direction. The top and bottom panels demonstrate that there is little power on time scales of 10 sec and 0.1 sec, whereas the middle panel shows a great deal of power on time scales of 1 sec. This is summarized in Figure 14 as a power spectrum.

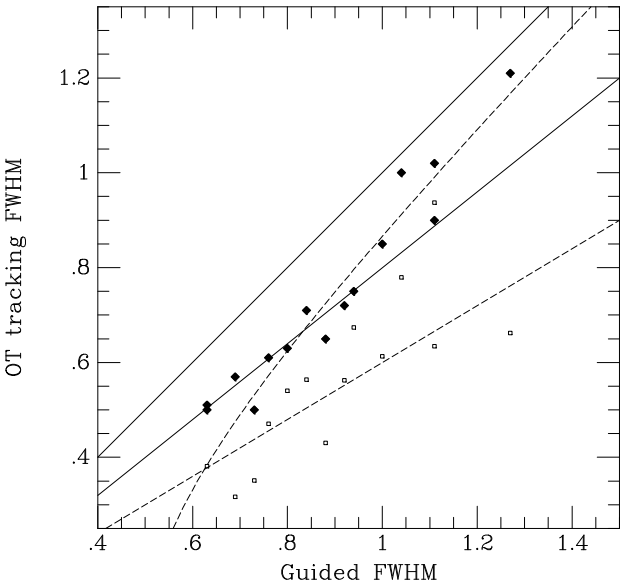

Fig. 10.— The PSF FWHM resulting from OT tracking is plotted against the FWHM from normal guiding (solid diamonds). The FWHM of the image motion (called α_G below) is shown as small open squares. The upper solid line is $y = x$, the lower solid line is $y = 0.8x$, the upper dashed line is $y = (x^2 - 0.5^2)^{1/2}$, and the lower dashed line is $y = 0.6x$.

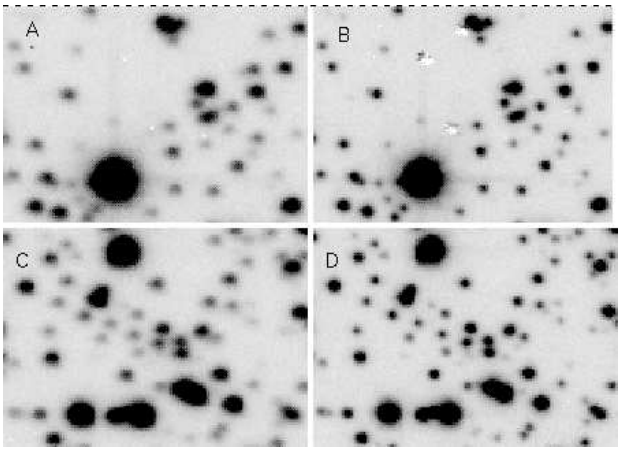

Fig. 11.— Two small portions of Figure 9 are shown in greater detail. The left images (A and C) are with ordinary tracking, the right (B and D) are with OT shifting, the upper images (A and B) are about 2′ from the guide star, and the lower images (C and D) are about 0.5′ from the guide star.

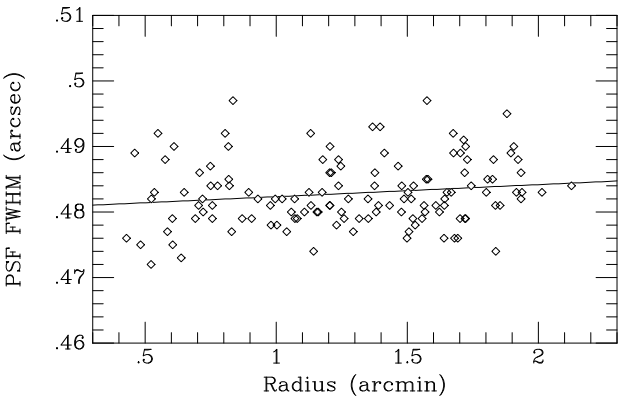

Fig. 12.— The PSF FWHM is shown as a function of distance from the guide star. The line is a formal fit to the data, but the data are consistent with no variation at all.

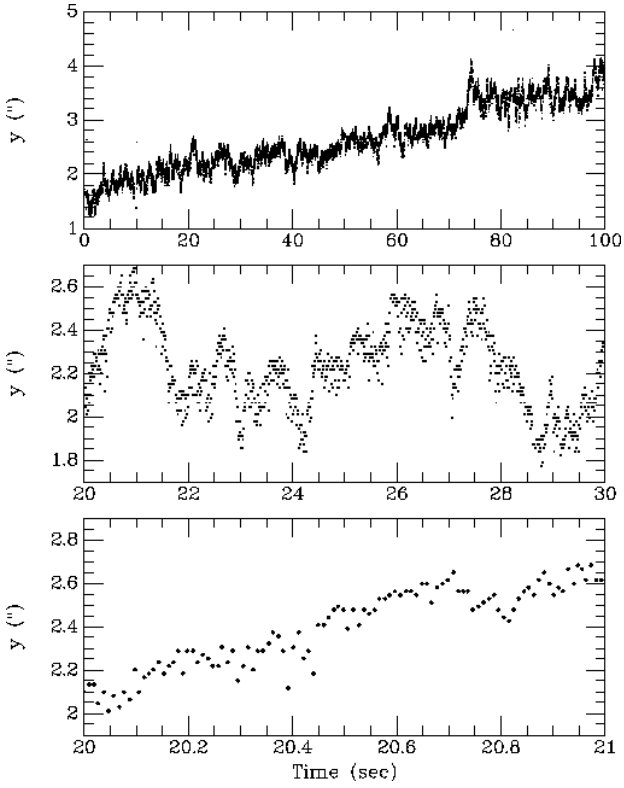

Fig. 13.— A time series of image motion in one direction is plotted against time for three different time intervals. The greatest power occurs on time scales of roughly 1 sec.

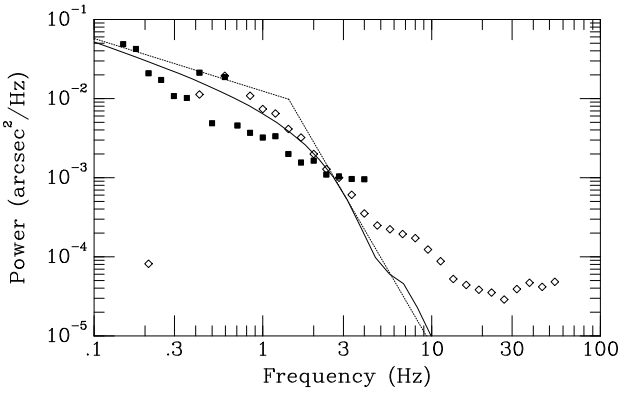

Fig. 14.— The power spectra of 1-axis image motion (with contributions from positive and negative frequencies summed) is plotted against frequency for two observations. The solid points were derived in the I band during seeing of about $0.7''$ (note the spikes at 0.4 and 0.6 Hz caused by autoguider error), and the open points were V band observations in $0.85''$ seeing. The centroiding has an RMS error of about 0.1 pixel which causes a noise floor around 10^{-4} arcsec^2/Hz. The curves are from an actual integration of the theoretical power spectrum using a Hufnagel-Valley model for C_n^2 scaled to $0.7''$ seeing along with a Bufton wind profile (solid line), and the broken power law approximation to it (dotted line). Most of the power occurs at $f \approx 1$ Hz where the power spectrum becomes steeper than f^{-1}. (The abcissa is log Hz, but the ordinate is power per Hz, not per log Hz.)

4.2. Kolmogorov Turbulence

The structure function of the atmospheric turbulence which causes image distortion must be integrated over the entire atmosphere, and the net amount of distortion is usually characterized in terms of the Fried parameter $r_0 = [0.423(2\pi/\lambda)^2\mu_0]^{-3/5}$, where μ_0 is the 0^{th} moment of C_n^2: $\mu_m = \sec^{m+1}\xi \int dh\, h^m\, C_n^2(h)$ (ξ is the zenith angle). The FWHM of the resulting image is then approximately $\alpha = \lambda/r_0$ (e.g. Racine 1996). Two other quantities of interest are the 1-axis tilt variance, given by $\sigma_G^2 = 0.5 \times 5.675\, D^{-1/3}\, \mu_0$, and its power spectrum $S(f)$ (Sasiela and Shelton 1993, and Tyler 1994). Combining the expressions for α and σ_G^2, evaluating at $\lambda = 650$ nm, and expressing the results in terms of arcseconds, we find that the 1-axis FWHM of the image motion, α_G, can be expressed in terms of the overall FWHM as

$$\alpha_G = 0.61 \left(\frac{\lambda}{650\text{nm}}\right)^{1/6} \left(\frac{2.4\text{m}}{D}\right)^{1/6} \alpha^{5/6}.$$

This is shown on Figure 10, and is not a bad match to the observed image motion. Subtracting this in quadrature is likewise not a bad match to the OT-tracking FWHM, although this may be somewhat fortuitous because we believe there is a contribution of about $0.4''$ to the FWHM from astigmatism.

The dependence of image motion on telescope aperture is remarkably weak. A 10-m telescope will have image motion whose FWHM is 0.5 of the overall seeing. The frequency will be lower than a 2.4-m telescope by a factor of 4, which makes it less obvious to the eye and more possible for an autoguided telescope to follow it. On the other hand it is possible that a 10-m telescope could do worse because of its greater moment of inertia.

Sasiela and Shelton also calculate the tip/tilt

variance between two stars as a function of separation angle, and this is illustrated in Figure 15 for a Hufnagel-Valley (HV; see Sasiela and Shelton Appendix B for references and formulae) parametrization of C_n^2 which has been scaled to give FWHM= $0.5''$. The eventual asymptote is $2.35 * 2^{1/2} * 0.145''$, square root of 2 times the FWHM motion of a single star, α_G, and correcting one star's motion by the other will improve the image as long as the differential motion is less than half of this. This calculation predicts differential motion at a separation of $2'$ of $0.12''$ FWHM in the perpendicular direction and $0.15''$ in the parallel direction, which would lead to images of $0.495 \times 0.505''$ at the edge of the chip. This is a more rapid degradation than is seen in Figure 12, and suggests that the turbulence occurs lower than the standard HV profile.

Finally, we can calculate the expected power spectrum for our observations, which depends not only on C_n^2 but also on the wind profile $v(h)$, under the "frozen turbulence" assumption, whereby the wind blows a stationary pattern of phase distortions across the telescope aperture. It is not difficult to match the power spectrum reasonably well by adjusting the wind profile (we use the standard Bufton (1973) profile, with a ground wind speed of 10 m/s), as seen in Figure 14. For this wind profile, half of the variance occurs at frequencies less than $f = 0.2$ Hz. Of course, in order to reduce the tilt jitter to less than the diffraction limit of the telescope, it is necessary to operate at much higher frequencies, but this demonstrates that even fairly slow tracking can remove most of the atmospheric image motion. Unfortunately most autoguiders have effective 3dB points at a small fraction of a Hz, partly because of slow sample rates but mainly because of the large inertia of the

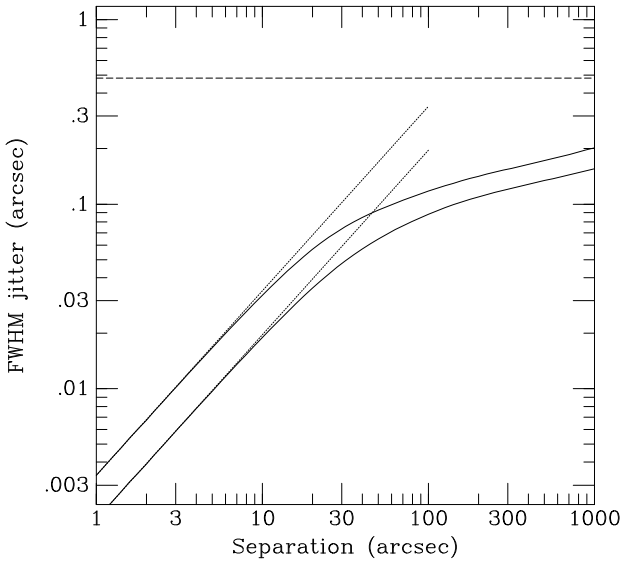

Fig. 15.— The theoretical FWHM 1-axis image motion (FWHM $\approx$ 2.4 RMS) of one star which is being shifted in accordance with the motion of another star, as a function of the separation of the stars. This uses a HV model for C_n^2 which has been scaled to $0.5''$ seeing. The upper curve is the motion in the radial direction between the stars and the lower curve is the tangential motion. The horizontal, dashed asymptote is $2^{1/2}$ times the jitter of one star. Note that the actual curves deviate very strongly on arcminute scales from the usual power law approximations which are accurate for small angles of separation (dotted lines).

telescope. A typical time scale for a telescope to get up to speed after an abrupt application of the drive motors is about 1 sec. This implies that $\omega_{3dB} \approx 2$ sec^{-1}, and $f_{3dB} \approx 0.3$ Hz. Without careful attention to the control loop, such a system will do a rather poor job of removing the image motion, even as slow as it is.

5. Conclusions

We have designed and built a new type of CCD which is capable of tracking image motion by shifting the developing electronic image to follow it. These first devices are 512×512 with an equal sized guide star area, which translates to a $1.5'$ field at the telescope. Characterization of these devices in the lab and observations at the MDM 2.4-m telescope indicate that they are indeed very effective at removing image motion.

The amplifiers achieve $1.6e^-$ noise at a responsivity of $16\mu\mathrm{V}/e^-$. The charge transfer efficiency is good enough (better than 0.999993) that a normal exposure consisting of thousands of shifts will not significantly degrade the PSF. The biggest concern about the effectiveness of these devices was the expectation that traps and pockets would dig holes in an image. However, this has proven not be be a serious problem. We do find that pockets are about three times more numerous under the OT gates than the three-phase gates, and we are suspicious that the use of aluminum for one of the gates has caused this enhancement in pockets.

Our observations using the device occurred during four nights when the seeing ranged from $0.6''$ to $1.3''$. We find that use of OT tracking sharpens images to approximately 80% of their normal size, or alternatively, OT tracking removes about $0.5''$ in quadrature from the image FWHM. The FWHM of image motion is roughly 60% of the FWHM of the PSF, and this is in good agreement with the Kolmogorov theory of turbulence. This theory predicts that image motion should be a very weak function of telescope aperture and its frequency goes inversely as telescope aperture (under the assumption of fixed wind speed from site to site), so removal of image motion is important for all telescopes.

We could match the power spectra of image motion quite well with Kolmogorov theory based on models of C_n^2 and the wind profile, and we found that the image motion is surprisingly slow. Most of the power occurs at frequencies of less than 1 Hz, but autoguiders moving a massive telescope may not have the bandwidth to remove much of this motion. However, OT tracking at 10 Hz or less removes virtually all of the image motion.

In contrast to Kolmogorov theory and these models, however, we observed no degradation of image quality as a function of distance from the guide star. The present device only permits us a range of about $2.5'$, but the models which successfully matched the power spectrum predict a fall-off in image quality which we did not observe. Therefore we believe that much of the contribution to our seeing comes from lower elevations, perhaps a boundary layer or even within the dome, and we expect that removal of image motion should be effective to quite large angles from the guide star, perhaps as large as $10'$.

Our development of a 512×512 OTCCD was based on the necessity to fit within the chords of wafers destined for another project, and on the expectation that image motion would become uncorrelated beyond about $2'$. Our hope for the future is to build a larger device, perhaps 2048×2048 with adjoining

guide star regions of 512×2048 because of the convenience and simplicity of being able to perform the entire job of sensing and compensating for star motion with one standard set of CCD electronics.

This research was supported by NSF grant AST-9314665.

REFERENCES

Beckers, J.M. 1993, ARA&A, 31, 13.

Burke, B.E., Reich, R.K., Savoye, E.D., & Tonry, J.L. 1994, IEEE Trans. Electron Devices, 41, 2482.

Bufton, J.L. 1973, Appl. Opt. 12 1785.

Chatterjee, P.K., Taylor, G.W., & Tasch, A.F. 1979, IEEE Trans. on Electron Devices, ED-26, 6, 871.

Cuillandre, J.-C., Fort, B., Picat, J.P., Soucail, G., Altieri, B., Beigbeder, F., Dupin, J.P., Pourthie T., Ratier, G., 1994, A&A, 281, 603.

Jacoby, G.H., Branch, D., Ciardullo, R., Davies, R.L., Harris, W.E., Pierce, M.J., Pritchet, C.J., Tonry, J.L., Welch D.L. 1992, PASP, 104, 599.

Kolmogorov, A.N. 1941, Dan. S.S.S.R., 30(4), 229.

McCarthy, J.K., Lu, B.W., Butcher, B.A., Behr, B.B., Jensen-Grey, S., Stubbs, C., Jim, K., & Brown, Y. 1997, PASP, in preparation.

McClure, R., Grundmann, W.A., Rambold, W.N., Fletcher, J.M., Richardson, E.H., Stillburn, J.R., Racine, R., Christian, C.A., & Waddell, P. 1989, PASP, 101, 1156.

Metzger, M.R., Tonry, J.L., & Luppino, G.A. 1993, ASP. Conf. Ser. 52, 300.

Parenti, R.R. & Sasiela, R.J. 1994, JOSAA, 11, 288.

Press, W.H., Teukolsky, S.A., Vetterling, W.T., & Flannery, B.P. 1992, *Numerical Recipes*, Second edition, Cambridge University Press: Cambridge

Racine, R. 1996, PASP, 108, 699.

Rigaut, F., Kern, P., Lena, P., Rousset, G., Fontanella, J.C., Gaffard, J.P., & Merkle, F. 1991, A&A, 250, 280.

Sasiela, R.J. & Shelton, J.D. 1993, JOSAA, 10, 646.

Schechter, P.L. et al. 1997, ApJ, 475, L85.

Sembach, K.R. & Tonry, J.L. 1996, AJ, 112, 797.

Stockman, H.S. 1982, SPIE Proc 331, 76.

Tatarski, V.I. 1961, "Wave Propagation in a Turbulent Medium", Dover:New York.

Thompson, L. & Ryerson, H.R. 1984, Proc. SPIE, 445, 560.

Tonry, J.L., Blakeslee, J.P., Ajhar, E.A., Dressler A., 1997, ApJ, 475, 399.

Tyler, G.A. 1994, JOSAA, 11,358.

This 2-column preprint was prepared with the AAS LaTeX macros v4.0.